JMEPEG (2017) 26:3058–3070
DOI: 10.1007/s11665-017-2779-3

1059-9495/$19.00

Effect of Cooling Rate on Microstructure and Mechanical Properties of Eutectoid Steel Under Cyclic Heat Treatment

Soma Maji, Amir Raza Subhani, Bijay Kumar Show, and Joydeep Maity

(Submitted November 13, 2016; in revised form May 22, 2017; published online June 15, 2017)

A systematic study has been carried out to ascertain the effect of cooling rate on structure and mechanical properties of eutectoid steel subjected to a novel incomplete austenitization-based cyclic heat treatment process up to 4 cycles. Each cycle consists of a short-duration holding (6 min) at 775 °C (above A_1) followed by cooling at different rates (furnace cooling, forced air cooling and ice-brine quenching). Microstructure and properties are found to be strongly dependent on cooling rate. In pearlitic transformation regime, lamellar disintegration completes in 61 h and 48 min for cyclic furnace cooling. This leads to a spheroidized structure possessing a lower hardness and strength than that obtained in as-received annealed condition. On contrary, lamellar disintegration does not occur for cyclic forced air cooling with high air flow rate (78 m^3 h^{-1}). Rather, a novel microstructure consisting of submicroscopic cementite particles in a 'inter-weaved pearlite' matrix is developed after 4 cycles. This provides an enhancement in hardness (395 HV), yield strength (473 MPa) and UTS (830 MPa) along with retention of a reasonable ductility (%Elongation = 19) as compared to as-received annealed condition (hardness = 222 HV, YS = 358 MPa, UTS = 740 MPa, %Elongation = 21).

Keywords cooling rate, cyclic heat treatment, eutectoid steel, lamellar disintegration, mechanical properties, microstructure

1. Introduction

Cyclic heat treatment that involves repeated thermal cycling around a critical temperature has been proved to cause many novel microstructural changes, thereby providing enhanced mechanical properties in steel. In early studies on steel, thermal cycling consisting of repeated α-γ phase transformations resulted in extensive grain refinement effect (Ref 1, 2). Thermal cycling around A_1 temperature resulted in an accelerated spheroidization (Ref 3-6). Besides, accelerated bainitic transformation is observed with cyclic austempering (Ref 7).

In recent years, a novel concept of incomplete austenitization-based cyclic heat treatment has been adopted by the research group of Maity (Ref 8-13). In this heat treatment process, each cycle consisted of holding for a short duration (6 min) in fully austenitic region (resulting in incomplete austenitization) followed by cooling to the room temperature in different cooling medium. In early approaches, cooling was carried out in a forced air medium with an air flow rate of 6 m^3 h^{-1} for 0.16 wt.% C, 0.6 wt.% C and 1.24 wt.% C steels. These research works envisaged many novel microstructural changes and improvement of material properties. A grain refinement effect was observed in 0.16 wt.% C steel (Ref 8). An accelerated spheroidization was identified in 0.6 wt.% C steel where the spheroidization process was completed only in 1 h 20 min with 8 cycles of heat treatment. This lead to a high ductility (%Elongation = 32) and modest strength (UTS = 727 MPa) (Ref 9-11). Furthermore, a combination of cementite spheroids and non-spheroids in α-ferrite matrix evolved in the microstructure of 1.24 wt.% C steel (Ref 12). This provided a high strength (UTS = 1086 MPa) coupled with relatively modest ductility (%Elongation = 13). In the next attempt (Ref 13), for further enhancement of strength, incomplete austenitization-based cyclic heat treatment was performed on AISI 1080 steel (eutectoid steel) with oil quenching (instead of forced air cooling). In this approach, on execution of three cycles, UTS was increased to 1609 MPa, though ductility was drastically reduced (%Elongation = 8). The noteworthy variation in microstructure and mechanical properties in these previously carried out investigations necessitates a systematic study on incomplete austenitization-based cyclic heat treatment process with regard to the effect of cooling rate. Accordingly, the present research work aims at: (i) carrying out a detailed study on the incomplete austenitization-based cyclic heat treatment of AISI 1080 steel (eutectoid steel) in view of the effect of cooling rate on microstructure (lamellar disintegration) and mechanical properties and (ii) obtaining a reasonable strength (UTS > 800 MPa) without any significant reduction in ductility as compared to annealed condition.

2. Experimental Procedure

The material selected for the present investigation was AISI 1080 steel (eutectoid steel). The chemical composition of this steel as analyzed by an optical emission spectrometer (WAS, FMSN: 01G 0026, Germany) is: 0.79 wt.% C, 0.73 wt.% Mn, 0.33 wt.% Si, 0.10 wt.% Cr, balance Fe. Initially, hot-rolled bars (dimension: 80 mm φ × 140 mm) of this steel were subjected to full annealing treatment at 775 °C for 1 h 20 min with furnace cooling (specimen code: AN). This

Soma Maji, Amir Raza Subhani, Bijay Kumar Show, and **Joydeep Maity**, Department of Metallurgical and Materials Engineering, National Institute of Technology Durgapur, Durgapur, West Bengal 713209, India. Contact e-mail: joydeep_maity@yahoo.co.in.

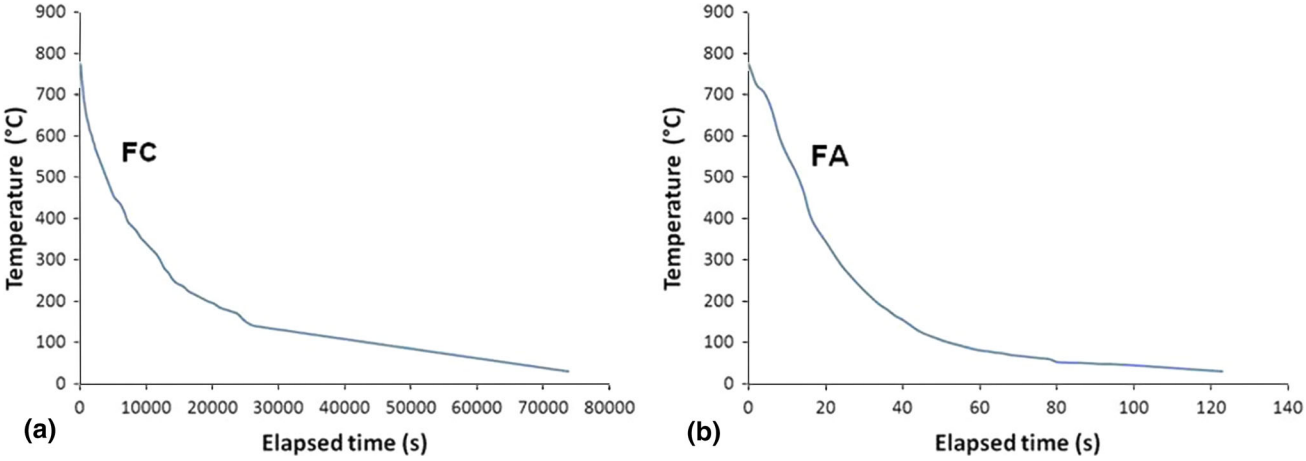

Fig. 1 Experimentally obtained cooling curves: (a) FC, (b) FA

Table 1 Duration of cyclic heat treatment processes

Type of cyclic heat treatment	Heat treatment code	Holding time	Cooling time	Duration of one cycle	Total duration of 4 cycles
Short-duration holding at 775 °C followed by furnace cooling	FC	360 s (6 min)	73,800 s	74,160 s	296,640 s
Short-duration holding at 775 °C followed by forced air cooling	FA	360 s (6 min)	123 s	483 s	1932 s
Short-duration holding at 775 °C followed by ice-brine quenching	IBQ	360 s (6 min)	Negligible	360 s	1440 s

annealed steel was considered as the as-received material for the present investigation. The bars of dimension 112 mm × 14 mm × 10 mm were machined out from the annealed steel bar and were subjected to incomplete austenitization (partial dissolution of cementite lamella in austenite)-based cyclic heat treatment up to 4 cycles. Each cycle consisted of inserting the specimen in an electric resistance furnace (temperature control accuracy = ±5 °C) in fully austenitic region at a temperature 775 °C (above the A_1 temperature) and holding for 6 min (short duration), followed by cooling in three different conditions to study the effect of cooling rate. Holding temperature and time being same, first set of specimens (code: FC) were subjected to furnace cooling (slowest possible cooling with an overall cooling rate of 0.01 °C s^{-1}), while second set of specimens (code: FA) were subjected to cooling in forced air (air flow rate = 78 m^3 h^{-1}; overall cooling rate = 6.06 °C s^{-1}) using an air blower. Furthermore, third set of specimens (code: IBQ) were subjected to quenching in ice-brine solution involving the fastest possible rate of cooling. It is important to note that air flow rate (78 m^3 h^{-1}) considered for forced air cooling in the present investigation was much higher than that (6 m^3 h^{-1}) adopted in previous investigations (Ref 8-12) carried out by the research group of present corresponding author. The temperature-time data during cooling in furnace and forced air were recorded using a digital thermometer (CIE, Model-305, Taiwan) consisting of a K-type thermocouple connected to a digital temperature recorder. The cooling curves so obtained for FC and FA are shown in Fig. 1(a) and (b). The overall cooling rate is ascertained by dividing the temperature drop [i.e., (775-30) °C] by the elapsed time in bringing down temperature from the holding temperature (775 °C) to room temperature (30 °C). The durations of two cyclic heat treatment processes for different cooling conditions are compared in Table 1.

The heat-treated specimens were sectioned to small pieces and subsequently subjected to standard metallographic polishing and etching (by 2% nital). These metallographic specimens were examined in an optical microscope (LEICA, DM-2500 M, Germany), scanning electron microscope (SEM, model: S-3000 N, Hitachi, Japan) and field emission scanning electron microscope (FESEM, model: Sigma HD, Zeiss, Germany). In view of quantitative metallographic analysis, the area percentage (stereologically equated to volume percentage) of divorced eutectoid region (DER) and pearlite region (PR) in the microstructure was determined by graphical point count method onto the optical micrographs (as per ASTM E562) considering 12 image frames. Since many significant smaller microconstituents (such as cementite spheroid, non-spheroidal cementite, which are often submicroscopic) were adequately resolved only in SEM/FESEM investigation (but not in optical metallography), quantitative analyses for these microconstituents were mainly carried out with SEM/FESEM micrographs. The sizes of the isolated cementite spheroids (CS) and non-spheroidal cementite particles (NC) in DER were measured from SEM/FESEM images at higher magnification. Furthermore, the ratio (R) of the area percentage of CS to the area percentage of NC in DER was evaluated from SEM micrographs. The sizes of isolated cementite particles were measured as an average of minor axis and major axis approximating individual particles as an ellipse in two dimension. The area percentages of cementite particles (either CS or NC) in DER were measured by graphical point count analysis of SEM

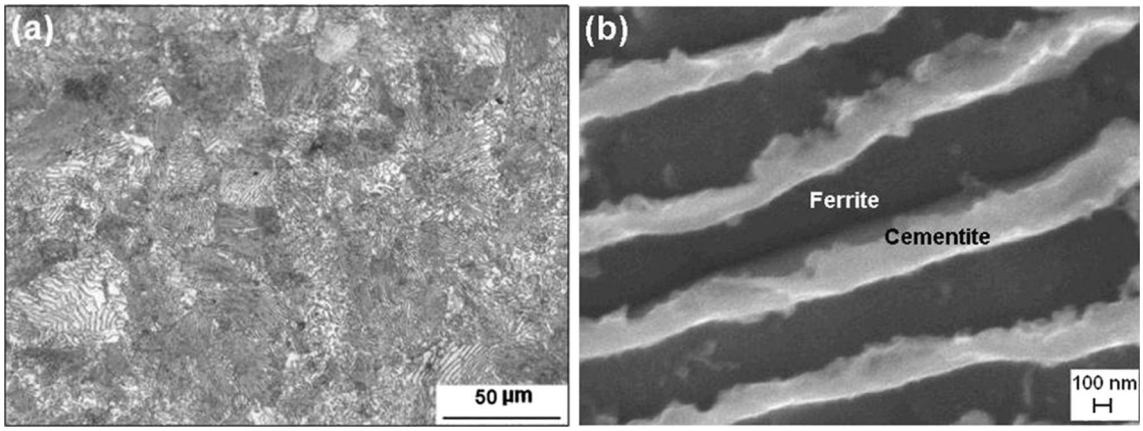

Fig. 2 Microstructure of as-received annealed AISI 1080 steel: (a) optical micrograph, (b) FESEM micrograph

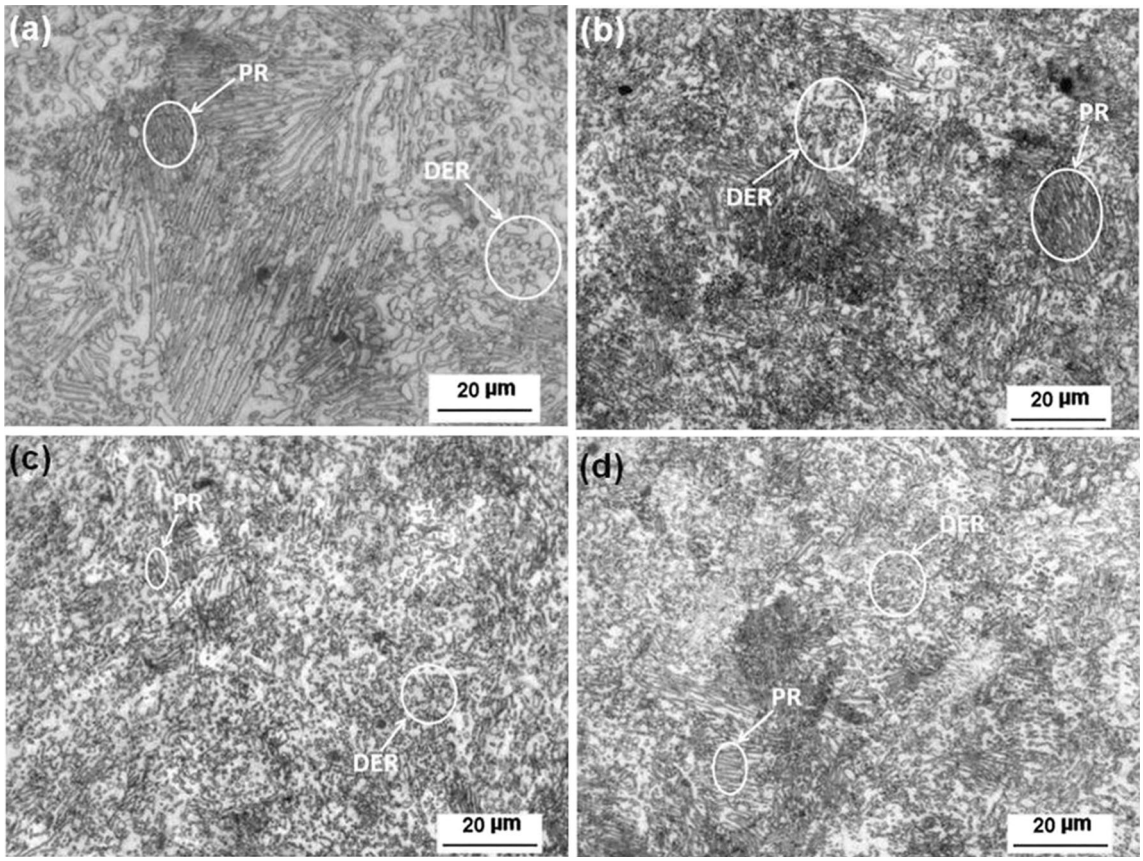

Fig. 3 Optical micrographs of AISI 1080 steel specimens subjected to cyclic furnace cooling: (a) FC-1 cycle, (b) FC-2 cycle, (c) FC-3 cycle, (d) FC-4 cycle

micrographs (considering 12 image frames for each specimen). Besides, interlamellar spacings in relevant micrographs were also measured from high-magnification SEM/FESEM images. In order to further identify different phases present, heat-treated AISI 1080 steel specimens were subjected to x-ray diffraction (XRD) analysis at slow scan rates in a high-resolution x-ray diffractometer (X'Pert PRO, PANalytical B.V., PW3040/60, the Netherlands) using Cu Kα radiation (λ = 0.15,406 nm). The overall phase analysis was carried out in a scan range: 2θ = 20°-90° at a scan rate of 0.5° min^{-1}. Besides, the presence of martensite was investigated through broadening/splitting of peak in a selected scan range: 2θ = 60°-70° at a scan rate of 0.25° min^{-1}.

In view of ascertaining mechanical properties, hardness values of the heat-treated specimens were measured in a Vicker's hardness testing machine (BV 250 (S), BIE, Miraj, India) using 30-kgf load. Furthermore, standard tensile test specimens (ASTM E 8 M) with 25 mm gauge length, 6 mm gauge width and 6 mm thickness were machined out from heat-treated steel bars and were subjected to tensile test in a

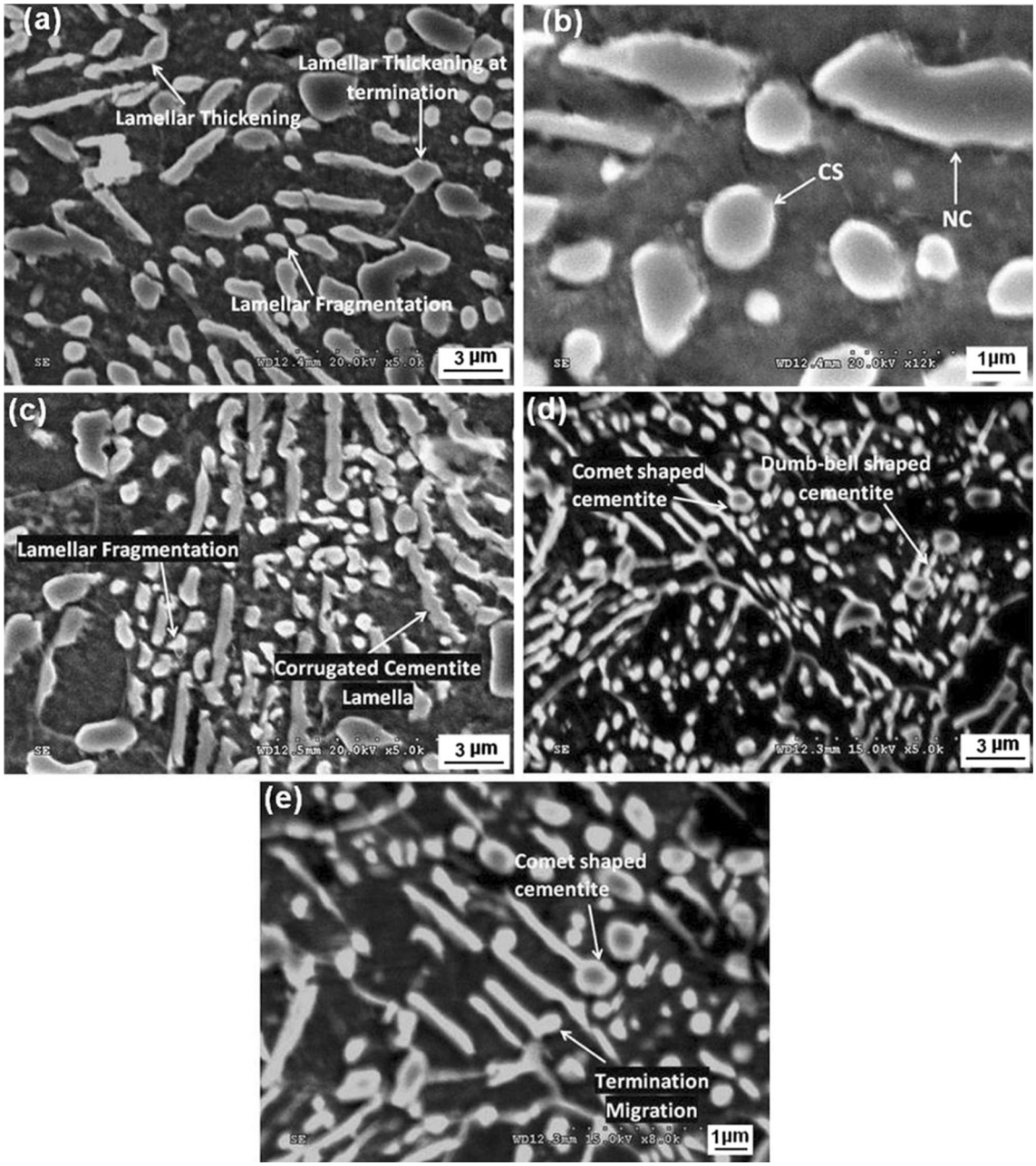

Fig. 4 SEM micrographs of AISI 1080 steel specimens subjected to cyclic furnace cooling at lower cycles: (a) FC-1 cycle (lower magnification), (b) FC-1 cycle (DER at higher magnification), (c) FC-1 cycle (pearlite region), (d) FC-2 cycle (lower magnification), (e) FC-2 cycle (higher magnification)

servohydraulic universal testing machine (INSTRON-8801, UK) of 100-kN capacity at a strain rate of 10^{-4} s^{-1}. Finally, fractured surfaces of the tensile tested specimens were examined in a field emission scanning electron microscope (FESEM, model: Sigma HD, Zeiss, Germany).

3. Results and Discussion

3.1 Evolution of Microstructure

The optical micrograph of as-received annealed AISI 1080 steel exhibits almost 100% pearlite (Fig. 2a). The lamellar morphology of pearlite is evident in the high-magnification FESEM micrograph (Fig. 2b).

Optical micrographs of the AISI 1080 steel specimens subjected to cyclic furnace cooling (FC) for different heat treatment cycles are shown in Fig. 3(a), (b), (c) and (d). High-magnification SEM and FESEM micrographs (for detailed analysis of microstructure and lamellar disintegration mechanism) of these specimens (FC) for different heat treatment cycles are shown in Fig. 4(a), (b), (c), (d) and (e) and 5(a), (b), (c) and (d). Unlike as-received full annealed steel, the presence of fragmented cementite (spheroid and non-spheroid) particles is identified in these micrographs. On a gross scale, the overall microstructure (as per Fig. 3a, b, c and d) consists of two

Table 2 Results of quantitative microstructure analysis from optical micrographs by graphical point count method for cyclic heat-treated specimens involving furnace cooling

Heat treatment schedule	Number of heat treatment cycles	Specimen code	Duration of heat treatment, s	% DER	% PR
Short-duration (6 min) holding at 775 °C followed by furnace cooling	1	FC-1 cycle	74,160	42	58
	2	FC-2 cycle	148,320	76	24
	3	FC-3 cycle	222,480	91	9
	4	FC-4 cycle	296,640	79	21

DER Divorced eutectoid region; *PR* pearlite region

Table 3 Results of quantitative microstructure analysis from high-magnification SEM micrographs for cyclic heat-treated specimens involving furnace cooling

Heat treatment schedule	Number of heat treatment cycles	Specimen code	Size of cementite spheroid, μm	Size of non-spheroid cementite particles, μm	R
Short-duration (6 min) holding at 775 °C followed by furnace cooling	1	FC-1 cycle	1.96 ± 0.49	2.64 ± 0.51	0.87
	2	FC-2 cycle	1.53 ± 0.46	1.89 ± 0.54	0.94
	3	FC-3 cycle	1.74 ± 0.41	1.99 ± 0.58	1.25
	4	FC-4 cycle	1.59 ± 0.31	1.94 ± 0.62	1.72

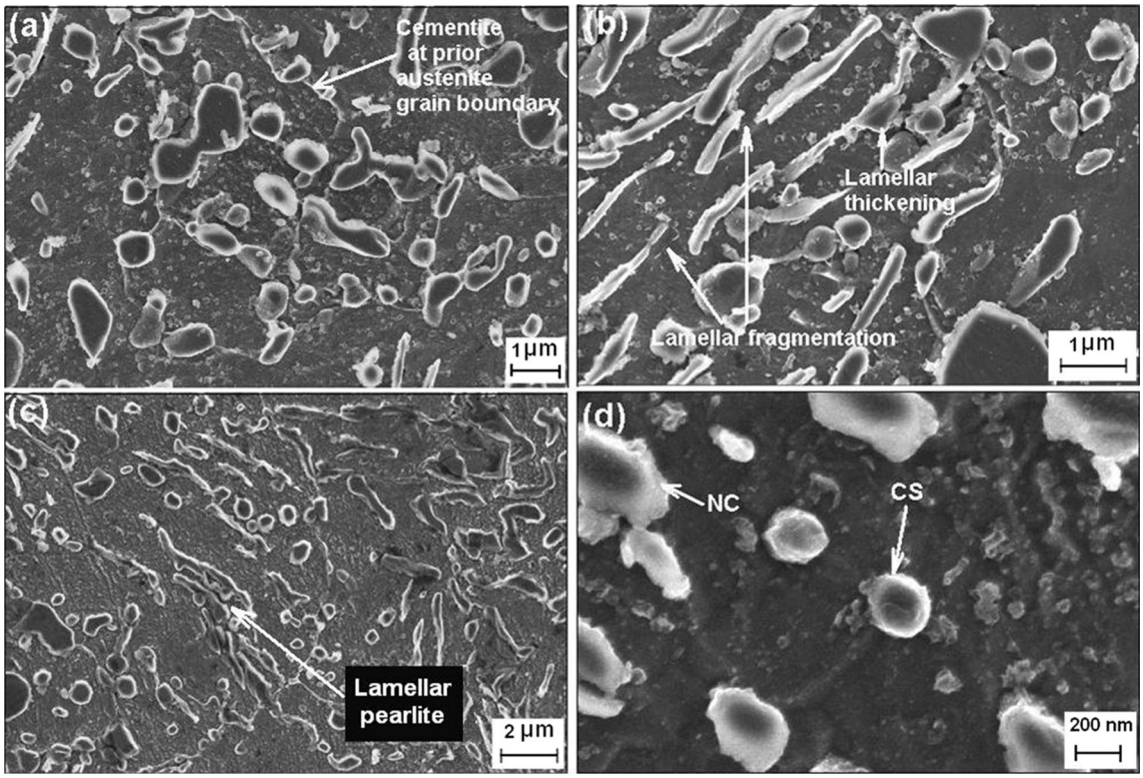

Fig. 5 FESEM micrographs of AISI 1080 steel specimens subjected to cyclic furnace cooling at higher cycles: (a) FC-3 cycle (overall microstructure), (b) FC-3 cycle (remaining pearlite region), (c) FC-4 cycle (lower magnification), (d) FC-4 cycle (DER at higher magnification)

distinct regions, namely (1) pearlite region (PR) and (2) divorced eutectoid region (DER). DER consists of fragmented cementite particles of different morphologies ('spheroid' and 'non-spheroid') in α-ferrite matrix. This region is the true indicative of lamellar disintegration which evolves through fragmentation of cementite lamella during short-duration

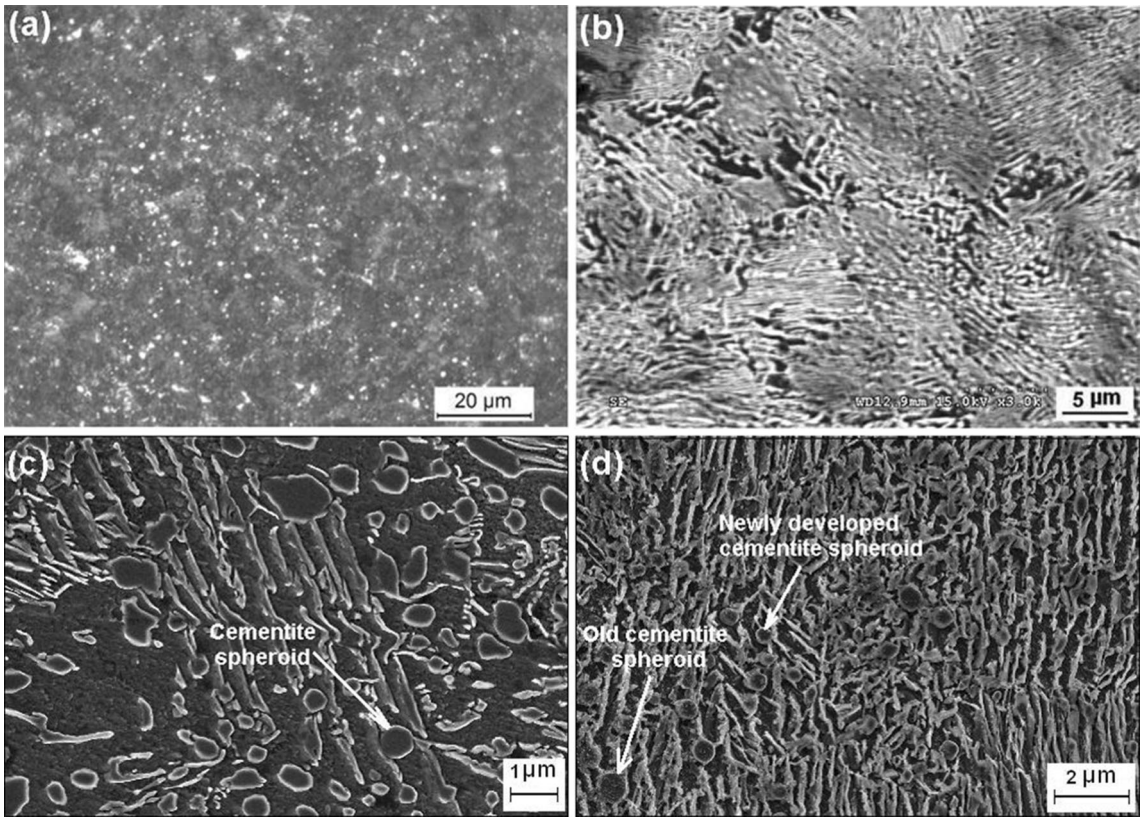

Fig. 6 Characteristic optical micrograph and lower-cycle SEM/FESEM micrographs of AISI 1080 steel specimens subjected to cyclic forced air cooling: (a) FA-4 cycle (optical micrograph), (b) FA-1 cycle (SEM lower magnification), (c) FA-1 cycle (FESEM higher magnification), (d) FA-2 cycle (FESEM higher magnification)

Table 4 Results of quantitative analysis from high-magnification SEM micrographs for cyclic heat-treated specimens involving forced air cooling

Heat treatment schedule	Number of heat treatment cycles	Specimen code	Size of new cementite spheroids, μm	Size of old cementite spheroids, μm	Interlamellar spacing (μm) of pearlite
Short-duration (6 min) holding at 775 °C followed by forced air cooling	1	FA-1 cycle	0.4 ± 0.09	Not applicable	0.58 ± 0.12
	2	FA-2 cycle	0.27 ± 0.07	0.68 ± 0.08	0.40 ± 0.10
	3	FA-3 cycle	0.22 ± 0.08	0.75 ± 0.13	0.28 ± 0.08
	4	FA-4 cycle	0.22. ± 0.07	0.61 ± 0.10	Not applicable (interweaved morphology)

(6 min) holding at high temperature (775 °C) followed by divorced eutectoid growth of fragmented cementite particles during cooling to the room temperature. The area percentages of PR and DER in these heat-treated FC specimens as evaluated from optical micrographs are presented in Table 2. Furthermore, the sizes of cementite spheroids (CS) and non-spheroidal cementite particles (NC) and the ratio (R) of the area percentage of CS to the area percentage of NC in DER as evaluated from SEM/FESEM micrographs are summarized in Table 3.

As per analysis of optical micrographs (Fig. 3a, b, c and d; Table 2), %DER increases and %PR decreases in FC specimens up to three heat treatment cycles indicating the progress of lamellar disintegration. In fact, lamellar disintegration almost attains completion (91% area of the microstructure containing DER) on execution of 3 cycles with a total duration of 61 h 48 min. This indicates relatively faster kinetics of lamellar disintegration under cyclic furnace cooling as compared to conventional spheroidization involving subcritical annealing [requiring a duration of 72-100 h (Ref 5, 6)]. DER is reduced to 79% on execution of the fourth cycle. This indicates the dissolution of some part of fine fragmented cementite particles into austenite while holding at 775 °C (for 6 min) and subsequent furnace cooling from 775 °C to 723 °C (requiring 6 min as per cooling curve, Fig. 1). This generates carbon-enriched austenite regions, which upon further cooling below 723 °C (A_1 temperature) transform into lamellar pearlite. Accordingly, PR is increased and DER is reduced in the microstructure after fourth cycle.

The high-magnification SEM image (Fig. 4a) exhibits a significant lamellar disintegration in FC specimen after single cycle of heat treatment. Evidences of 'lamellar thickening' (at termination as well in the body of cementite lamella through

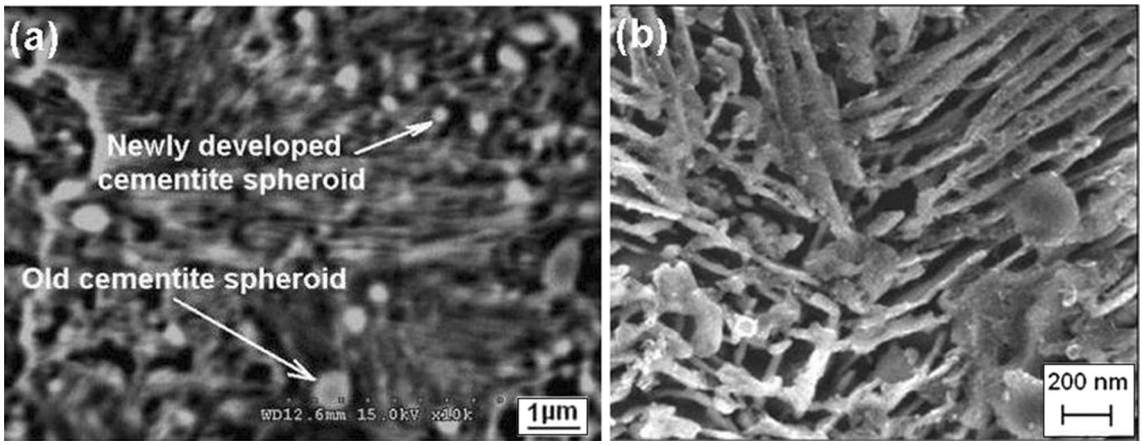

Fig. 7 Higher-cycle SEM and FESEM micrographs of AISI 1080 steel specimens subjected to cyclic forced air cooling: (a) FA-3 cycle (SEM micrograph), (b) FA-4 cycle (FESEM micrograph representing interpenetrating cementite lamella)

atomic diffusion within a cementite lamella from lamellar fault site to adjacent flat surface) and 'lamellar fragmentation' (through dissolution of cementite lamella into adjacent austenite at preferred sites of lamellar faults) are also visible. These phenomena cause evolution of isolated CS and NC (Fig. 4b) sizes which are quite coarse (Table 3) owing to substantial divorced eutectoid growth of fragmented cementite particles during slow furnace cooling (taking 20 h 30 min). In remaining pearlite region corrugated cementite lamellae are observed (Fig. 4c). This is a consequence of partial dissolution of cementite lamella at high-energy lamellar fault sites. This supports the philosophy of lamellar fragmentation occurring at preferred sites of lamellar faults as proposed by Maity et al. (Ref 11). Execution of second cycle leads to further lamellar disintegration through dissolution and fragmentation (Fig. 4d, e). The sizes of CS and NC appear to be much smaller than that obtained after first cycle (Table 3). This indicates intense fragmentation of remaining cementite lamella and partial dissolution of existing cementite particles during a total duration of 12 min above 723 °C. Besides, thickening at single termination of cementite lamella generating 'comet' shape, thickening at both the terminations of cementite lamella generating 'dumb-bell' shape (Fig. 4d, e) and termination migration (Fig. 4e) owing to prolong duration of cooling are readily visible. Lamellar disintegration almost achieves completion on execution of three cycles. More spheroids are originated (Fig. 5a) through intense lamellar fragmentation and subsequent divorced eutectoid growth during slow furnace cooling. Accordingly, *R*-ratio increases beyond 1 (i.e., 1.25) as per Table 3. Besides, cementite appears at prior austenite grain boundary predictably in the regions where carbon concentration locally exceeds 0.8 wt.% (thereby generating hypereutectoid composition) owing to dissolution of cementite in austenite during holding at 775 °C (Fig. 5a). In residual lamellar region, all usual processes, such as preferential dissolution of cementite at high-energy lamellar fault sites (lamellar fragmentation) and lamellar thickening at termination, are still in progress (Fig. 5b). Though lamellar disintegration is almost completed after 3 cycles, execution of another cycle (4th cycle) results in appearance of new lamellar pearlite region (Fig. 5c). Furthermore, the sizes of CS and NC in DER tend to decrease (Table 3). The origin of new pearlite region (PR) is a consequence of complete dissolution of smaller cementite particles (during holding at 775 °C and cooling up to 723 °C) forming carbon-enriched austenite regions. These regions, upon further cooling below 723 °C (A_1), transform into lamellar pearlite (Fig. 5c). Accordingly, PR is increased and DER is reduced in the microstructure (Table 2). On the other hand, partial dissolution of bigger cementite particles generates smaller CS and NC in DER (Fig. 5d).

As revealed in quantitative analysis of SEM micrographs (Table 3) for FC specimens, the *R*-ratio gradually increases with number of cycles. This is attributed to the fragmented cementite particles taking up the shape of spheroids through divorced eutectoid growth during very slow rate of furnace cooling. Slower cooling rate is expected to cause divorced eutectoid transformation at relatively higher temperature with lower degree of undercooling that would increase the probability for product phase (cementite) to take spheroid shape. Besides, the sizes of fragmented cementite particles (either spheroid or non-spheroid) in DER are greater than 1 μm. Furthermore, the size increases and decreases in alternate cycles depending on relative dominance of either 'lamellar fragmentation' or 'divorced eutectoid growth.' In case of furnace cooling, cooling rate being very slow, apart from 6 min of isothermal holding at 775 °C, subsequent cooling to 723 °C also accounts for 6 min. Accordingly, a total duration of 12 min in complete austenite region is available for 'lamellar fragmentation' that essentially occurs through atomic diffusion from fault site of cementite lamella (region of higher chemical potential) to adjacent austenite. Besides, subsequent cooling below 723 °C to the room temperature also takes a long time (20 h 24 min), providing a long time for divorced eutectoid growth. Therefore, the fragmented cementite particles obtaining large size through divorced eutectoid growth in one cycle would be reduced to smaller size in the next cycle due to lamellar fragmentation through partial dissolution. As a consequence, the sizes of cementite particles increase and decrease in alternate cycles.

A typical optical micrograph of AISI 1080 steel specimens subjected to cyclic forced air cooling (FA) for four cycles of heat treatment is shown in Fig. 6(a), where an apparent glimpse of fine cementite spheroids in a matrix of fine pearlite is visible. However, adequately resolved microstructures could only be observed under SEM and FESEM investigations (Fig. 6b, c, d and 7a, b). Although the duration of holding is short (6 min)

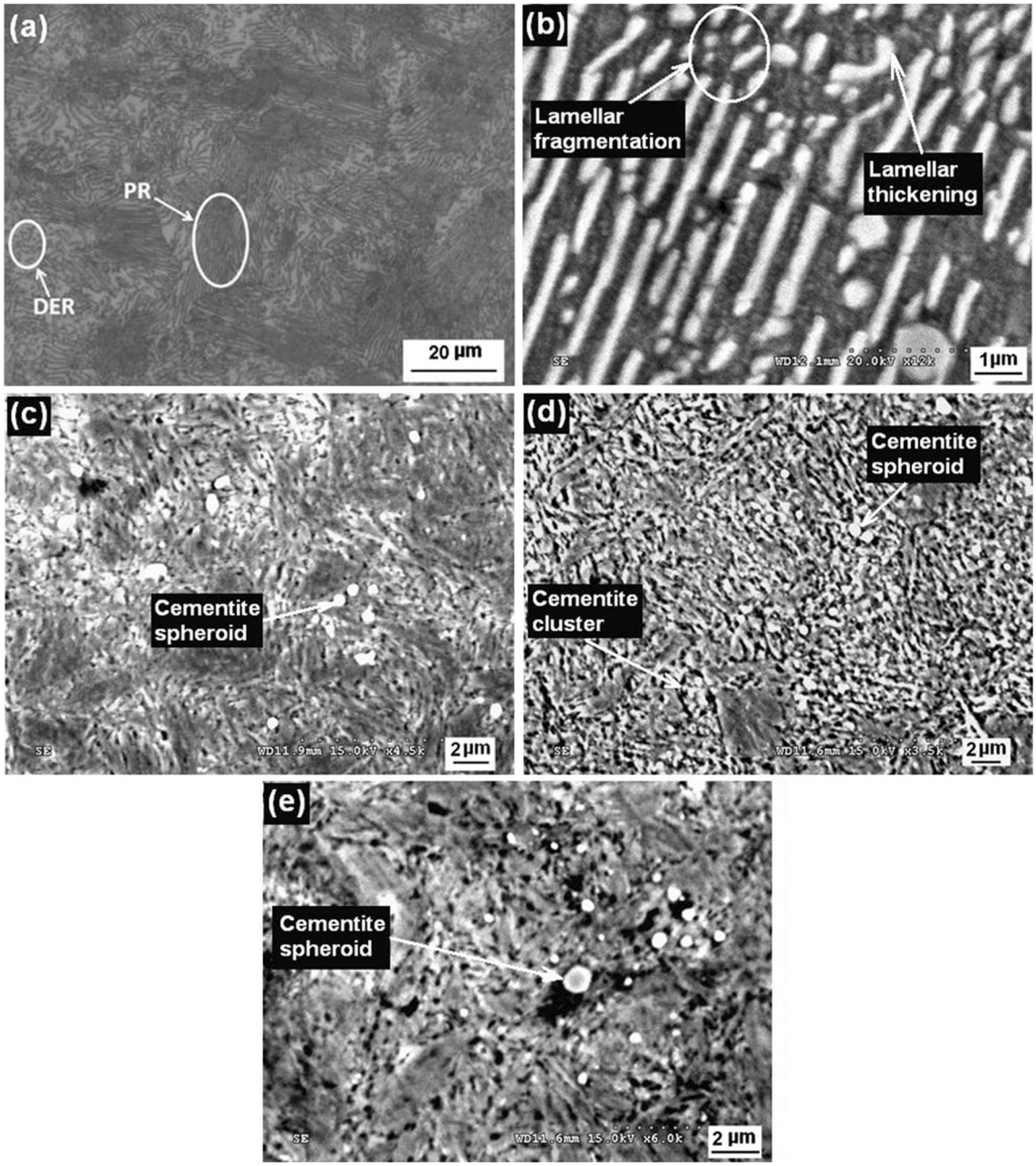

Fig. 8 Microstructure of AISI 1080 steel specimens subjected to cyclic ice-brine quenching: (a) IBQ-1 cycle (optical micrograph), (b) IBQ-1 cycle (SEM micrograph), (c) IBQ-2 cycle (SEM micrograph), (d) IBQ-3 cycle (SEM micrograph), (e) IBQ-4 cycle (SEM micrograph)

resulting in an incomplete dissolution of cementite in austenite, the cooling rate is very fast in reconstructive transformation regime under forced air cooling. Accordingly, in view of iron-carbon phase diagram, the eutectoid carbon content as well as eutectoid transformation temperature is lowered. As a consequence, even low carbon austenite regions transform into fully pearlitic structure, while fragmented cementite particles (originated through 'lamellar fragmentation') remain in the matrix in the form of spheroids. The sizes of the cementite spheroids are submicroscopic (less than 1 μm) (Table 4). Furthermore, the progress of cyclic heat treatment with FC results in divorced eutectoid growth of old spheroids (evolved in previous cycle) and origin of much finer submicroscopic new spheroids (Fig. 6d and 7a; Table 4). These new spheroids originate through further lamellar fragmentation above A_1 at highly dense lamellar fault sites developed in previous cycle during fast rate of cooling. As a consequence, the lamellar morphology of pearlite is gradually obscured. Finally, after 4 cycles of heat treatment, the matrix takes up 'interweaved pearlite' morphology (consisting of interpenetrating cementite lamella) along with the presence of extremely fine submicroscopic cementite particles (Fig. 7b). Such a novel microstructure, unlike other cases, cannot be categorized in terms of PR and DER. Furthermore, up to 3 cycles, interlamellar spacing of pearlite is also reduced with number of heat treatment cycles (Table 4).

Microstructures of AISI 1080 steel specimens subjected to cyclic ice-brine quenching (code: IBQ) are shown in Fig. 8(a), (b), (c), (d) and (e) and 9(a) and (b). Execution of single heat

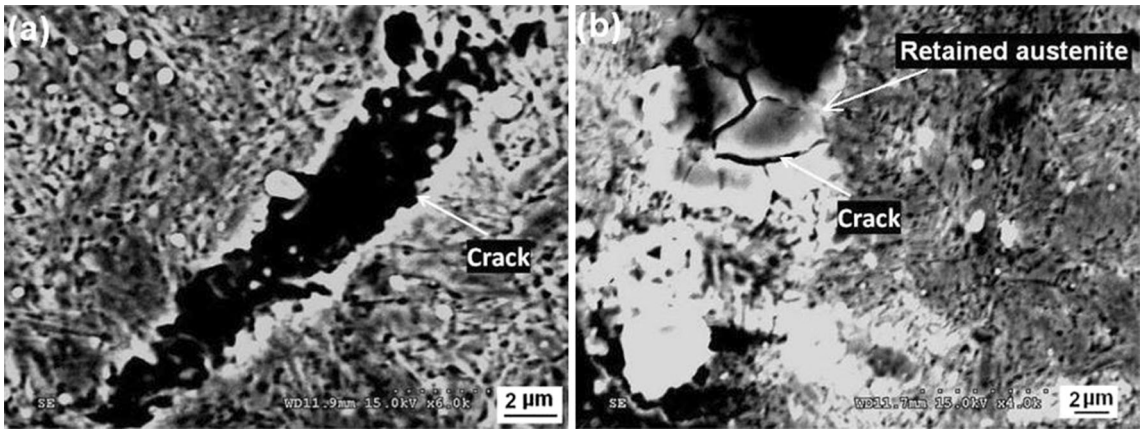

Fig. 9 Typical SEM micrographs of AISI 1080 steel specimens subjected to cyclic ice-brine quenching exhibiting the presence of quench crack: (a) IBQ-2 cycle, (b) IBQ-4 cycle

treatment cycle with IBQ results in the generation of 19% DER, while 81% region remains pearlitic as per graphical point count analysis onto optical micrograph (Fig. 8a). Furthermore, the high-magnification SEM image indicates initiation of lamellar disintegration process through lamellar fragmentation and lamellar thickening (Fig. 8b). Lamellar disintegration is completed on execution of the next cycle (second cycle) with a total duration of 12 min since extremely fast quenching in ice brine presumably generates highly defect enriched structure (both intense lamellar fault sites and matrix with high dislocation density) in first cycle. Accordingly, a structure consisting of 'fragmented cementite particles' (often spheroids) in martensite matrix is evolved (Fig. 8c). The sizes of fragmented cementite particles appear to be submicroscopic. On execution of third cycle, some fragmented cementite particles coalesce to form clusters. Consequently, microstructure contains isolated cementite particles and cementite clusters in martensite matrix (Fig. 8d). Execution of 4th cycle causes partial dissolution of cementite clusters in matrix (Fig. 8e).

Furthermore, repeated thermal cycling with extremely fast quenching in ice brine develops crack in the microstructure from second cycle onward (Fig. 9a). In particular, specimen subjected to 4 cycles of IBQ exhibits cracking in the location of retained austenite (Fig. 9b). A significant dissolution of carbon in austenite (thereby lowering the M_f temperature) on repeated holding at 775 °C results in the presence of retained austenite along with martensite upon quenching. The presence of retained austenite on execution of 4 cycles of IBQ is also confirmed with XRD analysis (to be discussed shortly).

The presence of different phases is further substantiated with x-ray diffraction analysis of heat-treated steels. X-ray diffractograms of selected specimens are shown in Fig. 10(a), (b), (c), (d), (e) and (f). The peaks of α-Fe and cementite (Fe_3C) are observed in majority specimens. In addition, the peak of γ-Fe is also obtained for IBQ-4 cycle specimen (Fig. 10f). The peaks of α-Fe indicate the presence of α-ferrite and martensite (for IBQ). α-Ferrite is present both as ferrite in pearlite (for AN, FC and FA) and as ferrite matrix in DER (in case of FC). The cementite phase is present in the form of lamellar cementite in pearlite (for AN, FC and FA) as well as the isolated spheroids and non-spheroids (in FC, FA and IBQ). In addition, the peak of γ-Fe in IBQ-4 cycle (Fig. 10f) indicates the presence of retained austenite. This is a consequence of lowering down the M_f temperature below room temperature owing to a significant dissolution of carbon in prior austenite on repeated holding at 775 °C followed by ice-brine quenching. The presence of martensite is further substantiated with the broadening of (002) peak of α-Fe for second cycle onward in case of IBQ (Fig. 10e, f). However, in other cases (AN, FC, FA and IBQ-1 cycle) sharp (002) peak of α-Fe indicates the presence of α-ferrite (Fig. 10a, b, c and d). In case of IBQ-1 cycle, the absence of (002) α-Fe peak broadening (Fig. 10d) indicates a matrix which is almost α-ferrite even after quenching. This is due to insufficient dissolution of carbon in prior austenite with only single-time short-duration (6 min) holding at 775 °C.

3.2 Mechanical Properties and Fractured Surface

The mechanical properties (hardness, yield strength (YS), ultimate tensile strength (UTS) and %Elongation) along with (UTS/YS) ratio of heat-treated specimens are graphically presented in Fig. 11(a) and (b). It is important to note that the tensile test was not carried out for second cycle onward for the specimens subjected to cyclic ice-brine quenching (IBQ) due to appearance of crack in the microstructure envisaging an expected premature failure of the specimens under tensile test. Annealed AISI 1080 steel [specimen code: AN, indicated as 0 cycle in Fig. 11(a) and (b)] possesses its characteristic modest hardness (222 HV) and strength (YS = 358 MPa, UTS = 740 MPa) along with a reasonable ductility (%Elongation = 21). Hardness and strength are attained by virtue of lamellar strengthening. Furthermore, quite a high (UTS/YS) ratio (2.07) is obtained due to coarse lamellar pearlitic structure. Such a structure ensures wider mean free path for dislocation motion resulting in a significant strain hardening of α-ferrite between two cementite lamellae.

The specimens subjected to cyclic furnace cooling (FC), for any number of heat treatment cycles, possess lower hardness and strength properties (YS and UTS) with a little higher ductility (%Elongation) as compared to as-received annealed steel. This is attributed to evolution of DER replacing PR on execution of cyclic furnace cooling. Fragmented cementite particles in DER being microscopic (>1 μm), the dispersion strengthening effect of DER (containing dispersed fragmented cementite particles in α-ferrite matrix) would not dominate over lamellar strengthening of PR. The occasional increase and

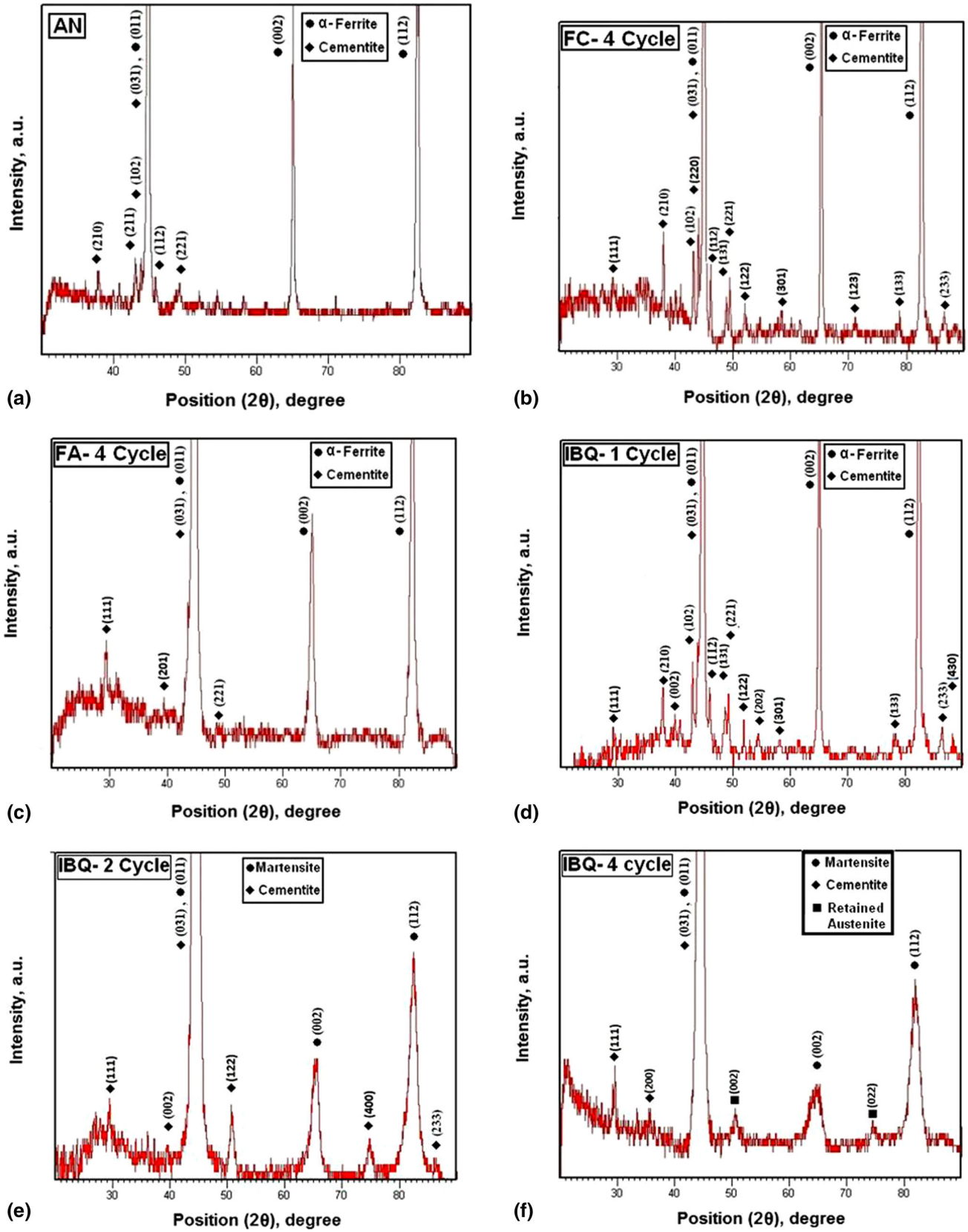

Fig. 10 X-ray diffractograms of selected heat-treated specimens: (a) AN, (b) FC-4 cycle, (c) FA-4 cycle, (d) IBQ-1 cycle, (e) IBQ-2 cycle, (f) IBQ-4 cycle

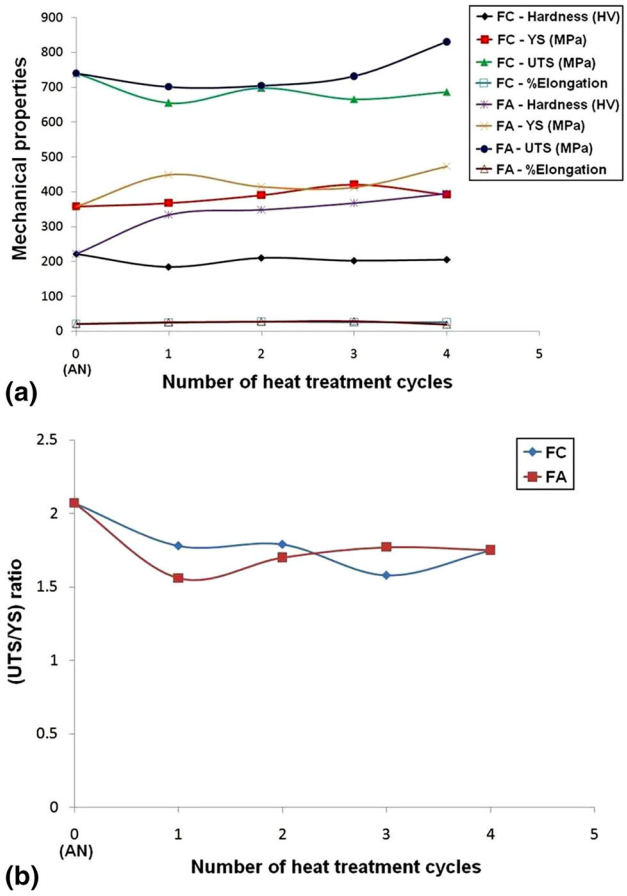

Fig. 11 Variation in (a) mechanical properties and (b) (UTS/YS) ratio of AISI 1080 steel specimens with heat treatment cycles

decrease in hardness and strength can be correlated with decrease or increase in the fragmented cementite particle size in DER. The FESEM fractographs of selected cyclic heat-treated tensile tested specimens are shown in Fig. 12(a), (b), (c) and (d). The FC specimens, in most cases, exhibit a mixed fracture mode that consists of the characteristic staircase cleavage facets in lamellar pearlite region and the presence of dimples in DER (Fig. 12a). These dimples are developed in DER through generation of microvoids at cementite particle-ferrite matrix interface and their coalescence. On execution of 3 cycles, as lamellar disintegration is almost completed (with the presence of 91% DER), the fractured surface mostly contains dimples (Fig. 12b).

On contrary, in case of cyclic forced air cooling (FA), for any heat treatment cycle, hardness and YS are higher than that of as-received annealed steel (AN). However, except 4 cycles of heat treatment, FA specimens possess lower UTS than AN. This is presumably attributed to inferior strain hardening behavior (as indicated by lower UTS/YS ratio) of FA as compared to AN. By virtue of much faster rate of cooling, FA specimens possess much smaller interlamellar spacings (Table 4) than AN specimen (Fig. 2) which reduces the mean free path for dislocation motion resulting in relatively inferior rate of strain hardening. Besides, in FA specimens, hardness and UTS increase with number of heat treatment cycles. This is presumably attributed to reduced interlamellar spacing and generation of much finer new submicroscopic cementite spheroids (Table 4) with progress of cyclic heat treatment promoting dispersion strengthening effect. The fractured surface (Fig. 12c) mainly contains staircase cleavage facets (corresponding to fine pearlite region) along with small dimples (consequent to the presence of submicroscopic cementite spheroids). Most importantly, on execution of 4 cycles of forced air cooling, a significant enhancement of hardness (395 HV), yield strength (473 MPa) and UTS (830 MPa) is observed with respect to AN. This is attributed to the evolution of a novel microstructure consisting of dispersed fine submicroscopic cementite particles in 'interweaved pearlite' matrix (containing interpenetrating cementite lamella) (Fig. 7b). Corresponding fractured surface exhibits cleavage facets along with small dimples (Fig. 12d). Crack propagation through interpenetrating cementite lamella develops cleavage facets. Small dimples are originated through microvoid coalescence at submicroscopic cementite spheroid-matrix interface. Furthermore, in a recent investigation, Yi et al. (Ref 14) added 1.93 wt.% Al in 0.78 wt.% C steel (near-eutectoid steel) followed by isothermal holding below A_1 (650 °C) so as to cause lamellar disintegration. However, though high ductility is obtained (%Elongation = 24), strength achieved is not so significant (UTS = 700 MPa). In another recent study, Lv et al. (Ref 15) applied a typical cyclic heat treatment on 0.8 wt.% C steel with each cycle consisting of a short-duration (5 min) holding at 770 °C (above A_1 temperature) followed by a short-duration (3 min) holding at 680 °C. Substantial ductility improvement (33.9% Elongation) was observed on execution of five cycles by virtue of spheroidization effect. However, strength attainment was not so significant (UTS = 650 MPa) as compared to the strength achieved (UTS = 830 MPa) in the present investigation after four cycles under cyclic forced air cooling.

In case of cyclic ice-brine quenching (IBQ), the hardness achieved in any cycle is higher than that obtained for AN. The hardness increases up to three cycles and thereafter decreases in fourth cycle. On execution of first IBQ cycle, hardness (273 HV) and strength (YS = 475 MPa, UTS = 687 MPa) achieved are relatively low along with a high ductility (%Elongation = 28). This is due to the presence of α-ferrite matrix as a consequence of insufficient dissolution of carbon in prior austenite with one-time short-duration (6 min) holding at 775 °C. This is reflected as an absence of (002) α-Fe peak broadening (Fig. 10d). However, second cycle onward, a huge improvement in hardness occurs due to origin of carbon-enriched martensite (martensitic strengthening) along with dispersed submicroscopic cementite particles (dispersion strengthening). However, tensile test for these specimens could not be performed due to appearance of quench crack in the structure. Extremely high hardness (1055 HV) is achieved on execution of third cycle where, in addition, cementite clusters appear in the microstructure along with submicroscopic cementite spheroids in a martensite matrix (Fig. 8d). On execution of fourth cycle, hardness decreases due to partial dissolution of cementite clusters and evolution of retained austenite (Fig. 8e, 9b and 10f).

4. Conclusions

1. Cyclic furnace cooling of annealed AISI 1080 steel provides relatively faster kinetics of lamellar disintegration (61-h 48-min duration) than conventional subcritical annealing (72-100-h duration).

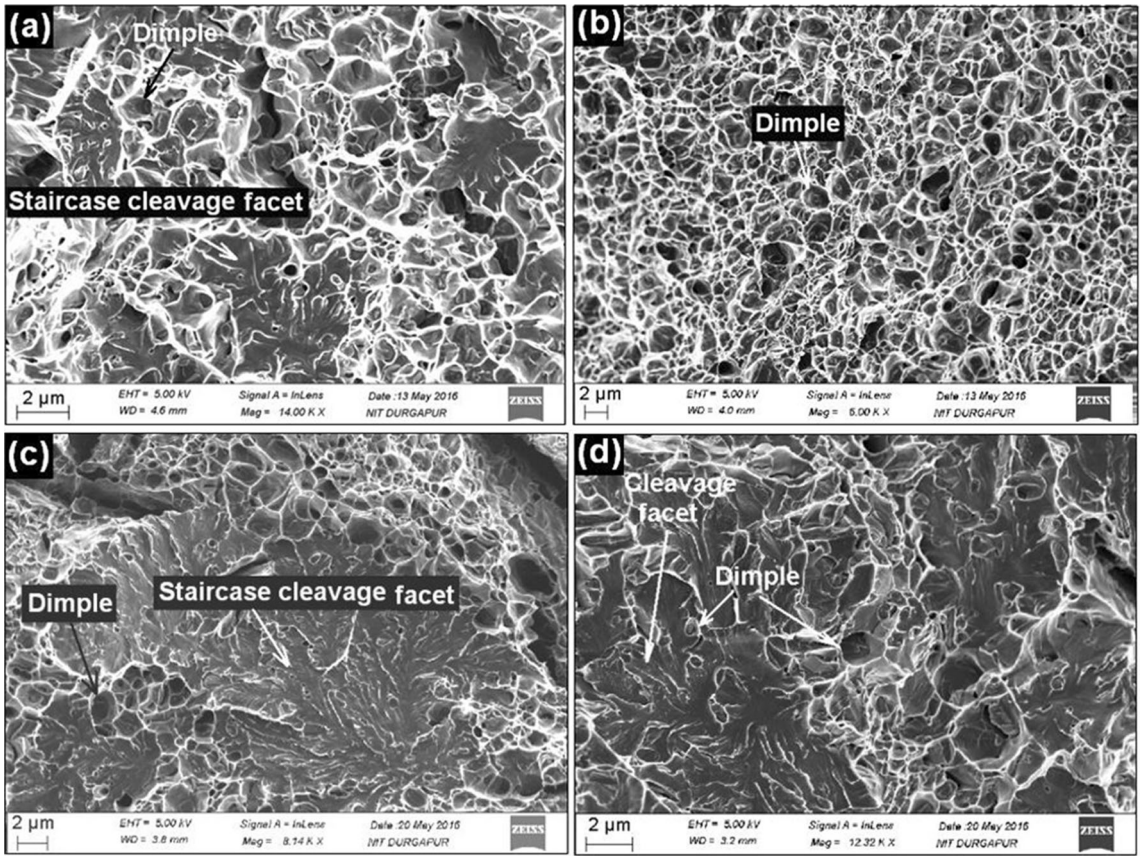

Fig. 12 FESEM fractographs of selected tensile tested specimens: (a) FC-1 cycle, (b) FC-3 cycle, (c) FA-1 cycle, (d) FA-4 cycle

2. On execution of cyclic furnace cooling to annealed AISI 1080 steel, the hardness and strength achieved in any cycle are lower than that obtained in as-received annealed condition (hardness = 222 HV, YS = 358 MPa, UTS = 740 MPa). This is attributed to the dominance of lamellar strengthening on dispersion strengthening effect of DER, since the sizes of cementite particles in DER are not submicroscopic. The occasional increase or decrease in hardness can be correlated with decrease or increase in fragmented cementite particle size.
3. On execution of cyclic ice-brine quenching to annealed AISI 1080 steel, lamellar disintegration achieves completion in 12-min duration. On execution of 3 cycles (18-min duration) exceptionally high hardness (1055 HV) is achieved with a microstructure consisting of submicroscopic cementite spheroids and cementite clusters in a martensite matrix. However, appearance of crack in the structure raises doubt on its application as a structural material.
4. Lamellar disintegration of annealed AISI 1080 steel does not occur on execution of cyclic forced air cooling with very high rate of air flow (78 $m^3\ h^{-1}$). Rather, a novel microstructure consisting of submicroscopic cementite spheroids in a 'interweaved pearlite' matrix is developed after 4 cycles. This provides a significant enhancement of hardness (395 HV), yield strength (473 MPa) and UTS (830 MPa) along with retention of a reasonable ductility (%Elongation = 19) with respect to as-received annealed condition.

References

1. R. Grange, Strengthening by Austenite Grain Refinement, *Trans. Am. Soc. Met.*, 1966, **1**, p 26–29
2. A. Anashkin et al., Heat Cycling of Carbon Steel Wire, *Met. Sci. Heat Treat.*, 1987, **2**, p 10–14
3. O.E. Cullen, Continuous Short-Cycle Anneal for Spheroidization of Cartridge-Case Steel, *Met. Prog.*, 1953, **64**, p 79–82
4. P. Payson, W.L. Hadapp, and J. Leeder, The Spheroidizing of Steel by Isothermal Transformation, *Trans. Am. Soc. Met.*, 1940, **28**, p 306–332
5. Y.L. Tian and R.W. Kraft, Mechanisms of Pearlite Spheroidization, *Metall. Trans. A*, 1987, **18A**, p 1403–1414
6. D.K. Mondal and R.M. Dey, Effect of Structures on the Response to Spheroidization in a Eutectoid Plain Carbon Steel, *Trans. IIM*, 1984, **37**, p 351–356
7. V. Sista, P. Nash, and S.S. Sahay, Accelerated Bainitic Transformation During Cyclic Austempering, *J. Mater. Sci.*, 2007, **42**, p 9112–9115
8. A. Saha, D.K. Mondal, K. Biswas, and J. Maity, Microstructural Modifications and Changes in Mechanical Properties During Cyclic Heat Treatment of 0.16% Carbon Steel, *Mater. Sci. Eng. A*, 2012, **534**, p 465–475
9. A. Saha, D.K. Mondal, and J. Maity, Effect of Cyclic Heat Treatment on Microstructure and Mechanical Properties of 0.6 wt% Carbon Steel, *Mater. Sci. Eng. A*, 2010, **527**, p 4001–4007
10. A. Saha, D.K. Mondal, and J. Maity, An Alternate Approach to Accelerated Spheroidization in Steel by Cyclic Annealing, *J. Mater. Eng. Perform.*, 2011, **20**, p 114–119
11. J. Maity, A. Saha, D.K. Mondal, and K. Biswas, Mechanism of Accelerated Spheroidization of Steel During Cyclic Heat Treatment Around Upper Critical Temperature, *Philos. Mag. Lett. Taylor & Francis*, 2013, **93**, p 231–237

12. A. Saha, D.K. Mondal, K. Biswas, and J. Maity, Development of High Strength Ductile Hypereutectoid Steel by Cyclic Heat Treatment Process, *Mater. Sci. Eng. A*, 2012, **541**, p 204–215
13. A. Mishra and J. Maity, Structure-Property Correlation of AISI, 1080 Steel Subjected to Cyclic Quenching Treatment, *Mater. Sci. Eng. A*, 2015, **646**, p 169–181
14. H.L. Yi, Z.Y. Hou, Y.B. Xu, D. Wu, and G.D. Wang, Acceleration of Spheroidization in Eutectoid Steels by the Addition of Aluminum, *Scr. Mater.*, 2012, **67**, p 645–648
15. Z.Q. Lv, B. Wang, Z.H. Wang, S.H. Sun, and W.T. Fu, Effect of Cyclic Heat Treatments on Spheroidizing Behavior of Cementite in High Carbon Steel, *Mater. Sci. Eng. A*, 2013, **574**, p 143–148